Asociación Argentina
de Mecánica Computacional

Mecánica Computacional Vol XXV, pp. 851-885
Alberto Cardona, Norberto Nigro, Victorio Sonzogni, Mario Storti. (Eds.)
Santa Fe, Argentina, Noviembre 2006

VORTEX-INDUCED VIBRATION (VIV) AROUND A CYLINDER AT LOW REYNOLDS NUMBERS: THE LOCK-IN PHENOMENON

German Filippini, Norberto Nigro, Mario Storti and Rodrigo Paz

Centro Internacional de Métodos Computacionales en Ingeniería (CIMEC) INTEC(CONICET-UNL), Güemes 3450, (S3000GLN), Santa Fe, Argentina, nnigro@intec.unl.edu.ar,
http://www.cimec.org.ar

Keywords: fluid-structure interaction, vortex-induced vibration, cylinder.

Abstract. In this paper some numerical results for vortex-induced vibrations (VIVs) of a cylinder at low Reynolds number are presented. The main goal of these preliminary results is the capturing of *synchronization/lock-in* phenomenon when Reynolds number is swept for low dimensionless mass ratio $(m^* \simeq 153.3524)$. This fluid-structure interaction problem (FSI) contains three main problems to be solved, the computational fluid dynamics (CFD), the computational mesh dynamics (CMD) and the multi-body dynamics (MBD). In this work this last problem is oversimplified to a single body dynamics, the cylinder. A stabilized ALE (Arbitrary Lagrangian-Eulerian) formulation is used to solve the incompressible laminar Navier Stokes equations. The cylinder is considered as a rigid body and it is free to vibrate along the vertical (transverse) direction and it is fixed to move in the horizontal one. The mesh dynamics may be solved in general by a global optimization strategy, however, in some special cases, a simple ad-hoc procedure may be adopted. For each sub-problem a second order accurate in time scheme is adopted. The fluid-structure interaction problem is solved with a strong coupling using a fixed point iteration strategy. It consists of an additional loop over the three problems forcing the convergence inside each time step. Hysteretic and vortex-shedding modes are two additional topics that deserve special attention and they are going to be included in a future work.

1 INTRODUCTION

The interaction of fluid flow with rigid body systems is often found in many areas of civil, mechanical and aerospace engineering. Moreover, in this context, the interaction between fluid and multibody systems may be regarded as a generalization of this topic, always included in a more general framework that belong to computational multiphysics.

The objective of this paper is merely the validation of the present implementation with some benchmarks. However the way in which the strong coupling is carried out deserves some additional discussion.

The main idea is based on the coupling between the fluid flow with sets of multibody systems that have translational and rotational degrees of freedom. Due to the complexity of the physical response of such systems, in the present work only simple tests are going to be presented. These problems have the attractive feature that they had been deeply analyzed by other researchers and they have an interesting physical behavior that deserves special attention. For example, a uniform fluid flow through an oscillating cylinder produces a vortex-induced vibration (VIV) that is very important for also engineering practice. The practical significance of vortex-induced vibration has led to a large number of fundamental studies, many of which are discussed in the comprehensive reviews Sarpkaya (1979); Griffin and S. (1982); Bearman (1984); Parkinson (1989); Blevins (1990); Naudascher and Rockwell (1993); Sumer and Fredsoze (1997) In the specific case of VIV around cylinders there are many papers Meneghini and Bearman (1995); Gabbai and Benaroya (2005); Khalak and Williamson (1999); Mittal and Tezduyar (1992); Singh and Mittal (2005); Nomura and Hughes (1992); Nomura (1994); Dettmer and Peric (2006) with contributions for the case of a oscillating cylinder only in the transverse direction or free to move in the two directions (transverse and in-line). This problem had been formulated for different approximation levels. One of them considers the problem as characterized by one or two dynamical systems, always one for the spring-mass cylinder is present and the other identifying the fluid behavior through a second order, in time, ordinary differential equation (ODE) may be added. In the former the fluid force is included through a forcing right hand side (rhs) term proportional to a combination of fluid displacements, velocities and accelerations. Each component of this forcing term is modeled arising algebraic coefficients extracted from experiments. In the latter, both ODE's have rhs terms that produce the two way coupling with coefficients that are chosen according to patterns observed from experiments. These semi-empirical models (like wake-oscillator model,*sdof*,force-decomposition models,variational approach) (Gabbai and Benaroya, 2005; Lu et al., 1996; Facchinetti et al., 2004) are very simple and they have additional advantages specially for high Reynolds numbers where direct numerical simulation is currently very difficult to use. Even though the coefficients may be extracted also from CFD, their evaluation is one of the main disadvantages for such a model. In the spirit of avoiding the difficulties associated with the modeling of turbulence and the necessity of calibrating coefficient with experiments, a CFD for low Reynolds number flows may be an interesting starting point to validate FSI with rigid body. Due to the high tendency to produce instabilities at the cylinder wake even at low Reynolds numbers, the VIV around cylinders is commonly solved at low Reynolds number.

In this work, only transverse oscillations of an elastically mounted rigid cylinder are analyzed. In (Khalak and Williamson, 1999) the influence of a low mass and damper system is studied. Fundamental questions concerning the vibration phenomena are included:

- the influence of the combined mass-damper parameter

- how the amplitude grows comforming the mass and damping ratio are lowered
- how is the response mode (wake vortex dynamics) and how about their jumps
- how the synchronization is defined

From the computational point of view the incompressible fluid flow is solved via a stabilized equal order velocity-pressure finite element formulation *streamline upwind / pressure-stabilizing/ Petrov Galerkin* method (SUPG-PSPG) (Tezduyar et al., 1992b) in a moving domain (Tezduyar, 1992). For linear interpolation this method may be regarded as a *Galerkin/least square* stabilization technique, commonly used in Eulerian finite element formulations in fluid-mechanics. An *arbitrary Lagrangian-Eulerian* (ALE) description is used to account for the deformation of the fluid domain arising from the displacement of the rigid bodies. Other alternative, not included here, is the space-time finite element formulation (Shakib, 1989) on moving domains, with several different implementations (Tezduyar et al., 1992c,d, 2006; Guler et al., 1999). The time integration for the fluid and the rigid body system is performed by a trapezoidal rule. In the former a second order Crank-Nicolson is commonly invoked and for the latter the second order system is split into two for displacement and velocity unknowns. Future improvements of this topic may be the usage of the *generalized* α-method (Jansen et al., 2000) for the fluid and some energy preserving integration scheme for the rigid body. To keep the second order while solving partitioned systems a second order predictor is added for the structural degrees of freedom when solving the fluid dynamics problem (Piperno and Farhat, 2001).

The coupling between these two systems is accomplished by an staged partitioned algorithm. It consists of an extra outer loop inside each time step that guarantees the convergence of the whole problem like a fixed point iteration over all the problems (Storti et al., 2006).

Beyond the physical and engineering importance, this problem is interesting from the computational point of view as a paradigm of multiphysics code implementation that reuses preexistent fluid and elastic solvers. The partitioned algorithm is implemented in the PETSc-FEM code (**`http://www.cimec.org.ar/petscfem`**) which is a parallel multi-physics finite element program based on the Message Passing Interface MPI and the Portable Extensible Toolkit for Scientific Computations PETSc. Two instances of the PETSc-FEM code simulate each subproblem and communicate interface forces and displacements via Standard C *FIFO* files or 'pipes'. The key point in the implementation of this partitioned scheme is the data exchange and synchronization between both parallel processes. These tasks are made in a small external C++ routine.

2 THE GOVERNING EQUATIONS

This special fluid-structure interaction problem needs to solve the fluid dynamics problem (CFD) coupled with the multi-body dynamics (MBD) and the computational mesh dynamics (CMD) in between. The next sections present each model problem making some emphasis in the continuum mechanics definition, the specific numerical solution for each subproblem, how to get a strong coupling feature with some flexibility for future software development and finally how to identify the main parameters that characterize the physical problem.

2.1 The moving reference frame

An essential feature of the problem under consideration is the interaction among the set of rigid bodies present in the system and the fluid flowing around them. This interaction takes place at the interface among the fluid and each rigid body or assembly of rigid bodies (multi-body). Because the fluid domain and the solid domains move arbitrarily it may be necessary to define a moving reference frame in which the conservation laws are formulated. This strategy is established through the arbitrary Lagrangian Eulerian *(ALE)* (Hughes et al., 1981; Belytschko et al., 1982; Donea et al., 1982) . Following (Dettmer and Peric, 2006) figure 1 shows the mapping and configurations commonly found in ALE formulation. The *initial* and the *current* configurations of the fluid body are represented by $\mathcal{B}_0$ and $\mathcal{B}$ respectively. Similarly, for the reference domain the initial and the current configurations are defined as Ω_0 and Ω. The material and spatial coordinate are $\mathbf{x}_0 \in \mathcal{B}_0$ and $\mathbf{x} \in \mathcal{B}$ respectively. The motion of the fluid body and the reference domain guarantees the existence of the following mapping:

$$\begin{aligned} \mathbf{x} &= \phi(\mathbf{x}_0, t) \\ \hat{\mathbf{x}} &= \lambda(\hat{\mathbf{x}_0}, t) \end{aligned} \tag{1}$$

Each $\mathbf{x} = \hat{\mathbf{x}} \in (\mathcal{B} \cap \Omega)$ is associated with a material point $\mathbf{x}_0$ and a reference point $\hat{\mathbf{x}}_0$ as illustrated in figure 1.

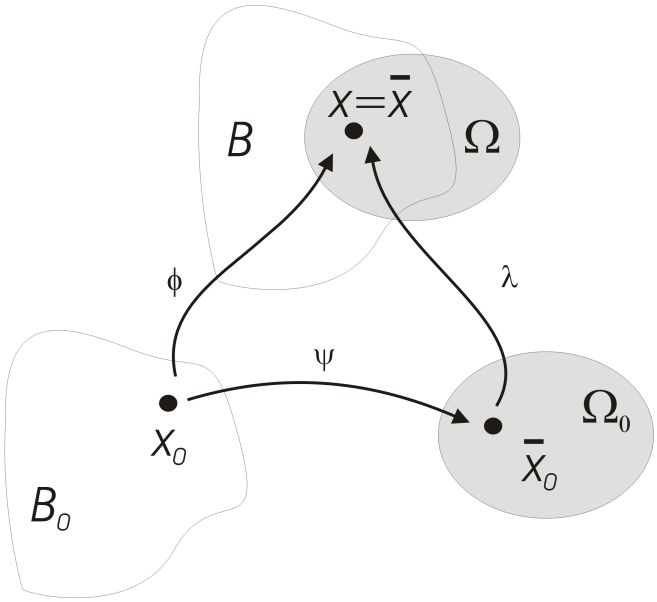

Figure 1: Mapping and coordinates in ALE formulation

Next, the *material* time derivative of $\mathbf{u}$ is obtained. The following relations among the different coordinate systems are valid:

$$\begin{aligned} \hat{\mathbf{x}}_0 = \psi(\mathbf{x}_0, t) = \lambda^{-1}(\phi(\mathbf{x}_0, t), t) \\ \mathbf{x} = \phi(\mathbf{x}_0, t) = \lambda(\hat{\mathbf{x}_0}, t) = \lambda(\psi(\mathbf{x}_0, t), t) = \hat{\mathbf{x}} \end{aligned} \tag{2}$$

Differentiation with respect to time for a specific constant material point $\mathbf{x}_0$ renders:

$$\frac{\partial \phi(\mathbf{x}_0, t)}{\partial t} = \frac{\partial \lambda(\hat{\mathbf{x}_0}, t)}{\partial t} + \frac{\partial \lambda(\hat{\mathbf{x}_0}, t)}{\partial \hat{\mathbf{x}}_0} \frac{\partial \psi(\mathbf{x}_0, t))}{\partial t} \tag{3}$$

Defining

$$\begin{aligned} \mathbf{u} &= \frac{\partial \phi(\mathbf{x}_0, t)}{\partial t} \\ \hat{\mathbf{v}} &= \frac{\partial \lambda(\hat{\mathbf{x}}_0, t)}{\partial t} \end{aligned} \tag{4}$$

So,

$$\frac{\partial \lambda(\hat{\mathbf{x}}_0, t)}{\partial \hat{\mathbf{x}}_0} \frac{\partial \psi(\mathbf{x}_0, t), t)}{\partial t} = \mathbf{u} - \hat{\mathbf{v}} \tag{5}$$

Expressing $\mathbf{u}$ in terms of the reference coordinate system,

$$\mathbf{u} = \hat{\mathbf{u}}(\hat{\mathbf{x}}_0, t) = \tilde{\mathbf{u}}(\hat{\mathbf{x}}, t) \tag{6}$$

therefore, the time derivative is achieved as:

$$\begin{aligned} \frac{D\mathbf{u}}{Dt} &= \frac{\partial \hat{\mathbf{u}}(\hat{\mathbf{x}}_0, t)}{\partial \hat{\mathbf{x}}_0} \frac{\partial \psi(\mathbf{x}_0, t))}{\partial t} + \frac{\partial \hat{\mathbf{u}}(\hat{\mathbf{x}}_0, t)}{\partial t} \\ &= \frac{\partial \tilde{\mathbf{u}}(\hat{\mathbf{x}}, t)}{\partial \hat{\mathbf{x}}} \frac{\partial \lambda(\hat{\mathbf{x}}_0, t)}{\partial \hat{\mathbf{x}}_0} \frac{\partial \psi(\mathbf{x}_0, t))}{\partial t} + \frac{\partial \hat{\mathbf{u}}(\hat{\mathbf{x}}_0, t)}{\partial t} \end{aligned} \tag{7}$$

Finally

$$\frac{D\mathbf{u}}{Dt} = \nabla_{\hat{\mathbf{x}}} \mathbf{u}(\mathbf{u} - \hat{\mathbf{v}}) + \mathbf{u}^{\cdot} \tag{8}$$

While the operator $\nabla_{\hat{\mathbf{x}}}(\cdot)$ denotes the derivative with respect to the current referential coordinates $\hat{\mathbf{x}}$, $\mathbf{u}^{\cdot}$ correspond to the change of the material particle velocity, noted by an observer travelling with the referential coordinate $\hat{x}_0$. (8) is sometimes called the *fundamental arbitrary Lagrangian-Eulerian equation*. The quantity $\mathbf{u} - \hat{\mathbf{v}}$ is commonly called the *convective velocity*.

2.2 Conservation equations

Viscous flow is well represented by Navier-Stokes equations. The incompressible version of this model includes the mass and momentum balances that can be written in the following form. Let $\Omega \in \mathbb{R}^{N_s p}$ and $(0, t_+)$ be the spatial and temporal fluid domains respectively, where $N_s p$ is the number of space dimensions, and let Γ be the boundary of Ω, both of them to be defined later. Therefore,

$$\begin{aligned} \nabla_{\hat{\mathbf{x}}} \cdot \mathbf{u} = 0 \quad &\text{in } \Omega \times (0, t_+) \\ \rho(\mathbf{u}^{\cdot} + (\mathbf{u} - \mathbf{v}) \cdot \nabla_{\hat{\mathbf{x}}} - \mathbf{f}) - \nabla_{\hat{\mathbf{x}}} \cdot \sigma = \mathbf{0} \quad &\text{in } \Omega \times (0, t_+), \end{aligned} \tag{9}$$

with ρ and $\mathbf{u}$ being the density and the velocity of the fluid, and σ the stress tensor, given by

$$\begin{aligned} \sigma &= -p\mathbf{I} + 2\mu^* \epsilon(\mathbf{u}) \\ \epsilon(\mathbf{u}) &= \frac{1}{2}(\nabla_{\hat{\mathbf{x}}} \mathbf{u} + (\nabla_{\hat{\mathbf{x}}} \mathbf{u})^t) \end{aligned} \tag{10}$$

where p is the pressure and μ^* is the effective dynamic viscosity defined as the sum of the dynamic (molecular) viscosity and the algebraic eddy viscosity coming from the turbulence model. $\mathbf{I}$ represents the identity tensor and ϵ the strain rate tensor.

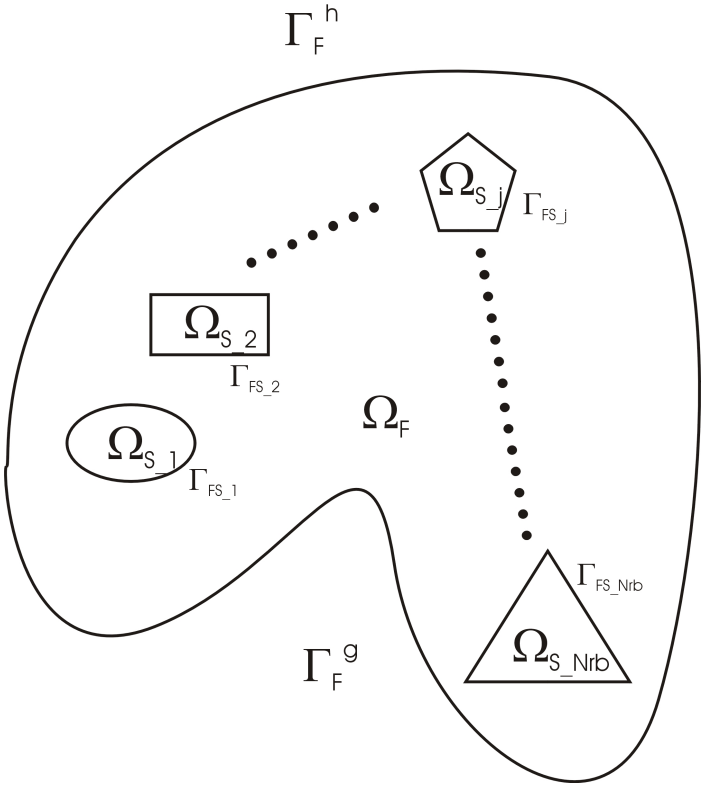

Figure 2: Partition of the domain for the fluid and multi-body and their interfaces

2.3 Initial and boundary conditions

In the last equation 9 the domain and its boundary were introduced in order to specify the support of the mathematical model. For fluid-structure interaction problems there are some details that need to be presented before introducing the boundary conditions. According to figure 2 it may be noted that:

$$\begin{aligned} \Omega &= \Omega_F \cup \Omega_S \\ \Omega_S &= \cup_j \Omega_{S_j} \\ \Gamma &= \Gamma_F \cup \Gamma_{FS} \\ \Gamma_{FS} &= \cup_j \Gamma_{FS_j} \end{aligned} \tag{11}$$

$$\begin{aligned} \Gamma_F &= \Gamma_F^g \cup \Gamma_F^h \\ \Gamma_{S_j F} &= \Gamma_{F S_j} \end{aligned}$$

with Ω_F the fluid domain, Ω_{S_j} the $j-th$ rigid body or set of rigid body (multi-body) where the rigid body dynamic problem is defined, Γ_F is the boundary wet by the fluid not lying at any rigid body interface, split in the Dirichlet and Neumann parts, and Γ_{FS_j}, is the boundary of the $j-th$ rigid body wet by the fluid.

Therefore, the boundary conditions are:

$$\begin{aligned} \mathbf{u} - \mathbf{g} &= \mathbf{0} \ \forall (\hat{\mathbf{x}}, t) \in \Gamma_F^g \times I \\ \sigma \cdot \hat{\mathbf{n}} - \mathbf{h} &= \mathbf{0} \ \forall (\hat{\mathbf{x}}, t) \in \Gamma_F^h \times I \\ \mathbf{u} - \mathbf{d}^{\cdot} &= \mathbf{0} \ \forall (\hat{\mathbf{x}}, t) \in \Gamma_F S \times I \\ (\mathbf{u} - \hat{\mathbf{v}}) \cdot \hat{\mathbf{n}} &= 0 \ \forall (\hat{\mathbf{x}}, t) \in \Gamma_F S \times I \end{aligned} \tag{12}$$

where $\mathbf{g}, \mathbf{h}, \hat{\mathbf{n}}$ denote the prescribed velocity, the traction vectors and the current outward normal unit vector of the boundary respectively.

The last two conditions third condition in 12 represent the no-slip condition at the fluid-rigid body interface Γ_{FS}. The fourth equation guarantees that the reference frame accurately represents the current configuration of the rigid body.

The forces $\mathbf{F}$ and the moments $\mathbf{M}$ are computed by the following expressions:

$$\begin{aligned} \mathbf{F} &= -\int_{\Gamma_{FS}} \sigma \cdot \hat{\mathbf{n}} d\Gamma \\ \mathbf{M} &= -\int_{\Gamma_{FS}} \Delta\mathbf{x} \times \sigma \cdot \hat{\mathbf{n}} d\Gamma \end{aligned} \tag{13}$$

where $\Delta\mathbf{x}$ means the current relative position of a point lying on the surface of the rigid body with respect to its gravity center G.

Finally the following initial conditions are included: $\mathbf{u} = \mathbf{u}_0$, $\mathbf{u}^{\cdot} = \mathbf{u}_0^{\cdot}$ and $\hat{\mathbf{x}} = \hat{\mathbf{x}}_0 \ \forall \hat{\mathbf{x}} \in \Omega$ at $t = 0$.

2.4 Rigid body dynamics

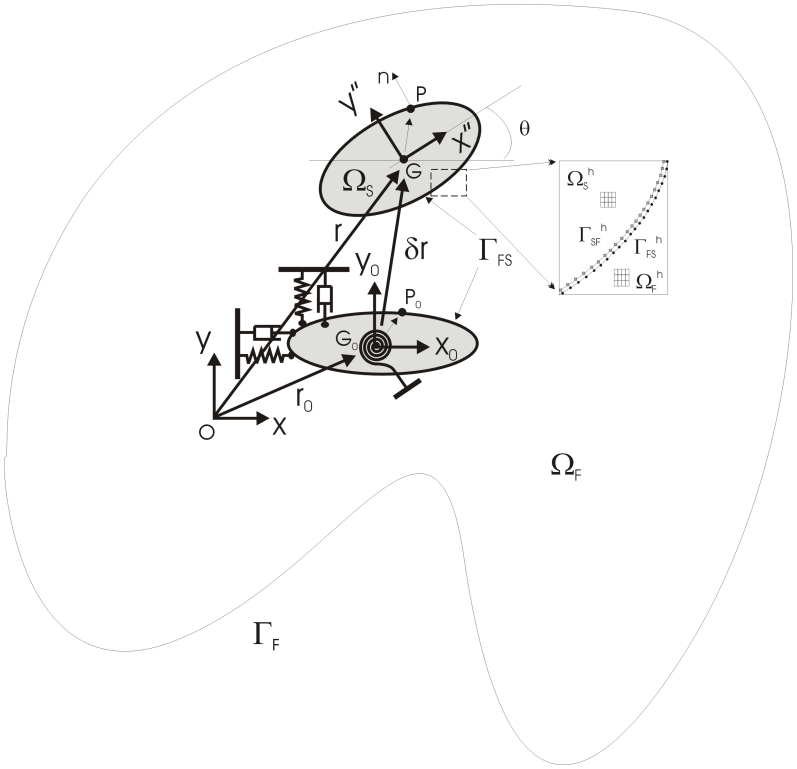

Figure 3: Rigid body dynamics problem

In order to simplify the presentation a set of rigid bodies in a two dimensional situation is considered. Extensions to the three-dimensional case is standard in specific bibliography. Multi-body case is left for future work. Each rigid body has a set of three equations associated with the 3 *dof'*sfor 2D, two for each components of the linear momentum conservation (d_i) and the reminder accounts for the conservation of angular momentum (θ). Linear and angular inertia, damping and stiffness characterize the rigid body motion assuming for simplicity that the behavior is linear and uncoupled.

$$\begin{aligned} m_i^k d^{\cdot\cdot k}_i + c_i^k d^{\cdot k}_i + k_i^k d_i^k = F_i^k \\ I_\theta^k \theta^{\cdot\cdot k} + c_\theta^k \theta^{\cdot k} + k_\theta^k \theta^k = M^k \end{aligned} \tag{14}$$

where i means the coordinate direction x, y and k is an index along the whole set of rigid bodies. The displacements d_i^k are the components of the k rigid body translation whereas θ^k describes the k rigid body orientation. In this paper the rotational dynamics is not included, therefore we drop this equation in the further discussion.

A typical description of the rigid body dynamic problem may be viewed in figure 3. The initial position of a typical rigid body is defined through the center of mass G_0, located relative to an inertial reference frame (X, Y) by position vector $\mathbf{r}_0$, and the body fixed reference frame (X_0, Y_0). A typical point at its surface is named P_0 By the fluid forces and moments the rigid body moves to the current position defined by G, with the new position vector $\mathbf{r} = \mathbf{r}_0 + \delta\mathbf{r}$ and its new orientation given by (X', Y') rotated from the original orientation an angle θ. The point P_0 moves to its current location P with the new normal $\mathbf{n}$.

The motion of the rigid body surface can be related to the degrees of freedom of its center of mass G. The motion of the rigid body surface is the input for the mesh dynamics stage of the computation. It also influences the fluid solver through the temporal term $(GCLlaw)$ and through the convective velocity $(\mathbf{u} - \hat{\mathbf{v}})$. Therefore it is necessary to know how each discrete node belonging to the wet interface between the fluid and the rigid body moves. This movement arises naturally from the hypothesis of rigid body, as a combination of a translation with the center of mass and a rotation around it:

$$\mathbf{d}_{FS}^k = \tilde{\mathbf{d}}_{FS}(\mathbf{d}^k, \theta^k, \Delta\mathbf{x}_0^k) \tag{15}$$

where $\Delta\mathbf{x}_0$ describes the initial position of each discrete node lying at the surface of the rigid body with respect to its center of mass.

It should be remarked that it is necessary to identify the center of mass of each rigid body and also each rigid body surface mesh and its mapping with the corresponding fluid surface mesh. In this work both surfaces at the interface are identical so it is not necessary to do any interpolation. Therefore each rigid body is defined with its center of mass and a surface mesh. To generalize the treatment two meshes are adopted, the fluid mesh that may be arbitrary (triangles or quadrangles) and the rigid body mesh that is generated by each panel at the surface joined to the center of mass. This mesh is ficticious because it is only used to define relative positions among each surface node and the center of mass G. A detail of the two meshes and the interface is shown in figure 4

2.5 The mesh dynamics

In general the computational mesh dynamics (CMD) problem is solved via a global optimization strategy (Lopez et al., 2006) that shows a significant enhanced robustness relative to

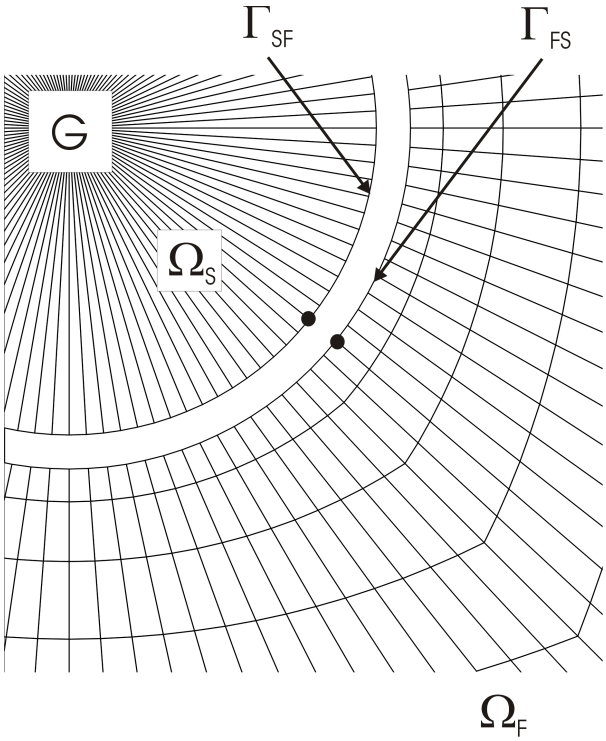

Figure 4: Meshes and discrete interfaces

the standard pseudo-elastic formulation for the mesh deformation (Tezduyar et al., 1992a; Johnson and Tezduyar, 1994). In this kind of problems this feature is very welcomed because the rigid body motion may be large enough to produce tangled (invalid) meshes. However, for some simple problems (like the vertical oscillating cylinder) an ad-hoc algorithm may be used with good results.

3 DIMENSIONLESS PARAMETERS

In order to identify the oscillatory response of the cylinder it is very attractive to rewrite the rigid body equations of motion, 14, using dimensionless variables. In this way it is clearly defined how the parameters should be chosen in order to get similarity among the experiments. In order to gain some theoretical insight about the influence of these dimensionless parameters on the behavior of the oscillator, some simple model for the fluid (like *wake oscillator models*) may be included. Starting with 14 considering for simplicity that only one rigid body is involved, and defining the following space and time reference scales:

$$\begin{aligned} \mathbf{X}_i &= \frac{\mathbf{d}_i}{D} \\ \tau = \frac{t}{t^{ref}} &= \frac{tU_\infty}{D} \end{aligned} \tag{16}$$

with little algebra it is possible to arrive to the following equation:

$$X_i^{\cdot\cdot} + 4\pi F_n \zeta X_i^{\cdot} + (2\pi F_n)^2 X_i = \frac{2C_i^x}{\pi m^*} \tag{17}$$

where $X_i^{\cdot} = \frac{\mathrm{d}X_i}{\mathrm{d}\tau}$, $X_i^{\cdot\cdot} = \frac{\mathrm{d}^2X_i}{\mathrm{d}\tau^2}$ are the dimensionless time derivative for each dimensionless spatial coordinate and C_i^x is the dimensionless force coefficient, commonly named *drag* and *lift*

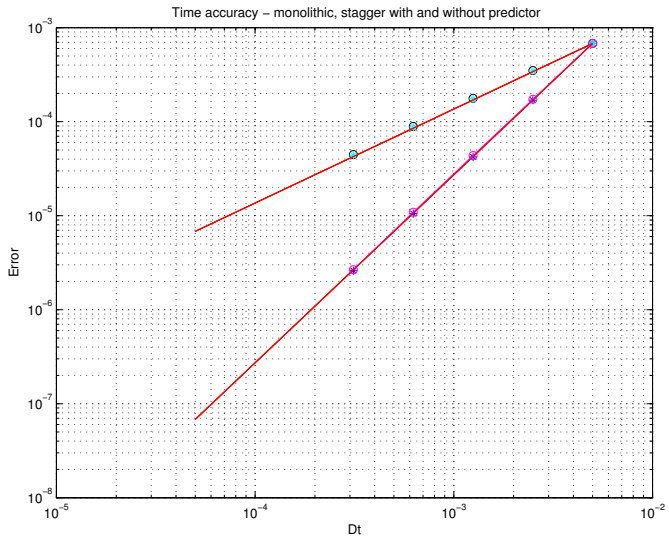

Figure 5: Time accuracy for staggered schemes. Influence of predictor.

coefficients. The dimensionless parameters that may be observed from 17 are:

- *mass ratio* $m^* = \frac{4m}{\pi \rho_\infty D^2 L}$
- *frequency ratio* $F_n = \frac{f_n D}{U_\infty}$
- *damping ratio* $\zeta = \frac{c}{2\sqrt{\kappa\, m}}$
- *Reynolds number* $Re = \frac{\rho U_\infty D}{\mu}$

The first three influence noticeably the behavior of the oscillating cylinder altering not only the Reynolds number where the lock-in phenomenon is achieved, also modifying the range of Reynolds numbers and the maximum oscillation amplitude during the lock-in. There are some other definitions for the reduced damping factor, one of them uses the sum of the fluid added mass to the rigid body mass instead of using only this last one.

4 STABILIZED FINITE ELEMENT FORMULATION FOR FLUID FLOW

In this work the solution of incompressible Navier-Stokes equations with the SUPG-PSPG method proposed by Tezduyar *et al.* (Tezduyar et al., 1992b) is implemented. SUPG ('*Streamline Upwind/Petrov Galerkin*') is used to stabilize the advection dominated terms and PSPG ('*Pressure Stabilizing/Petrov Galerkin*') is necessary to circumvent the checkerboard modes induced by the incompressibility constraint.

In this effort the solution of incompressible Navier-Stokes equations with an equal order pressure and velocity spatial discretization is used. As it is well known, in general this methodology does not satisfy the Babuska-Brezzi condition and it is necessary to stabilize the formulation through the addition of two operators. Advection at high Reynolds numbers is stabilized with the well known *SUPG* ('*Streamline Upwind/Petrov Galerkin*' operator, while the *PSPG* ('*Pressure Stabilizing/Petrov Galerkin*') operator stabilizes the incompressibility condition, which is responsible of the checkerboard pressure modes.

The computational fluid domain $\Omega = \Omega_F$ is divided in $N_e l$ finite elements Ω_e, $e = 1, \ldots, N_e l$, and let $\mathcal{E}$ be the set of these elements, and H^{1h} the finite dimensional space defined by

$$H^{1h} = \Big\{ \phi^h | \phi^h \in C^0(\overline{\Omega}), \phi^h|_{\Omega^e} \in P^1, \forall \Omega^e \in \mathcal{E} \Big\}, \tag{18}$$

with P^1 representing polynomials of first order. The functional spaces for the interpolation and weight functions are defined as

$$\begin{aligned} S^h_{\mathbf{u}} &= \{\ \mathbf{u}^h | \mathbf{u}^h \in (H^{1h})^{N_{sp}}, \mathbf{u}^h = \mathbf{g}^h \ \text{ on } \Gamma_g\ \} \\ V^h_{\mathbf{u}} &= \{\ \mathbf{w}^h | \mathbf{w}^h \in (H^{1h})^{N_{sp}}, \mathbf{w}^h = \mathbf{0} \ \text{ on } \Gamma_g\ \} \\ S^h_p &= \{\ q | q \in H^{1h}\ \}. \end{aligned} \tag{19}$$

The SUPG-PSPG scheme is written as follows: *Find* $\mathbf{u}^h \in S^h_u$ *and* $p^h \in S^h_p$ *such that*

$$\begin{aligned} &\int_\Omega \mathbf{w}^h \cdot \rho\Big(\frac{\partial \mathbf{u}^h}{\partial t} + \mathbf{u}^h \cdot \nabla \mathbf{u}^h\Big) + \int_\Omega \epsilon(\mathbf{w}^h) : \sigma^h d\Omega + \\ &+ \underbrace{\sum_{e=1}^{nel} \int_\Omega \delta^h \cdot \Big[\rho(\frac{\partial \mathbf{u}^h}{\partial t} + \mathbf{u}^h \cdot \nabla \mathbf{u}^h) - \nabla \cdot \sigma^h\Big] +}_{\textit{(SUPG term)}} \\ &+ \underbrace{\sum_{e=1}^{nel} \int_\Omega \epsilon^h \cdot \Big[\rho(\frac{\partial \mathbf{u}^h}{\partial t} + \mathbf{u}^h \cdot \nabla \mathbf{u}^h) - \nabla \cdot \sigma^h\Big] +}_{\textit{(PSPG term)}} \\ &+ \int_\Omega q^h \nabla \cdot \mathbf{u}^h d\Omega = \int_{\Gamma_h} \mathbf{w}^h \cdot \mathbf{h}^h d\Gamma \qquad \forall \mathbf{w}^h \in V^h_u\,,\ \forall q^h \in V^h_p \end{aligned} \tag{20}$$

where the stabilization parameters in equation (20) are defined as

$$\begin{aligned} \delta^h &= \tau_{\mathrm{SUPG}} (\mathbf{u}^h \cdot \nabla) \mathbf{w}^h \\ \epsilon^h &= \tau_{\mathrm{PSPG}} \frac{1}{\rho} \nabla q^h \\ \tau_{\mathrm{PSPG}} &= \tau_{\mathrm{SUPG}} = \frac{h_{\mathrm{elem}}}{2||\mathbf{u}^h||} z(Re_u). \end{aligned} \tag{21}$$

Note that the SUPG and the PSPG terms are defined on different functional spaces. These stabilizations terms act, at the linear system level by adding nonzero values on the diagonal entries associated with the pressure equations. The Reynolds number Re_u based on the element parameters is

$$Re_u = \frac{||\mathbf{u}^h|| h_{\text{elem}}}{2\nu}, \tag{22}$$

the element size h_{elem} is computed as (Tezduyar and Park, 1986),

$$h_{\text{elem}} = 2\Big(\sum_{a=1}^{nn} |\mathbf{s}\cdot\nabla N_a|\Big)^{-1} \tag{23}$$

being N_a the shape function associated with the node a, nn the number of nodes in the element, and $\mathbf{s}$ a unit vector on the streamline direction. The function $z(Re)$, appearing in 21, is defined as

$$z(Re) = \begin{cases} Re/3 & 0 \le Re < 3 \\ 1 & 3 \le Re \end{cases} \tag{24}$$

5 TIME INTEGRATION

Applying the stabilized finite element spatial interpolation a semidiscrete set of ordinary differential equations in time arise. Though, temporal discrization is needed in order to solve the problem. Here, a trapezoidal rule is used for both, the fluid and the rigid body equation using the parameters in such a way to obtain second order accurate in time.

For the fluid the final fully discretized systems is written as:

$$\begin{aligned} \mathbf{M}\frac{\mathrm{d}\mathbf{u}}{\mathrm{d}t} + \mathbf{A}(\mathbf{u})\mathbf{u} &= \mathbf{F}^{rb-f}(t,\mathbf{d}) \\ \mathbf{M}\frac{\mathbf{u}^{n+1}-\mathbf{u}^n}{\Delta t} + \mathbf{A}(\mathbf{u}^{n+\alpha})\mathbf{u}^{n+\alpha} &= \mathbf{F}^{rb-f}(t^{n+\alpha},\mathbf{d}^{n+\alpha}) \end{aligned} \tag{25}$$

with $\alpha = \frac{1}{2}$ for second order accuracy in time. $\mathbf{F}^{rb-f}$ is the generalized forcing term exerted by the rigid body over the fluid, in this case associated with the rigid body surface displacements. 25 is a simplification of the real equations because the mass matrix $\mathbf{M}$ and the system matrix $\mathbf{A}$ are both dependent of the rigid body displacements and velocities through the ALE formulation.

The rigid body equation of motion are written as a system of two first order equations:

$$\begin{aligned} m_i \ddot{d}_i + c_i \dot{d}_i + k_i d_i &= F_i^{f-rb} \\ \begin{pmatrix} 1 & 0 \\ 0 & m_i \end{pmatrix} \frac{\mathrm{d}}{\mathrm{d}t}\begin{pmatrix} d_i \\ \dot{d}_i \end{pmatrix} + \begin{pmatrix} 0 & -1 \\ k_i & c_i \end{pmatrix}\begin{pmatrix} d_i \\ \dot{d}_i \end{pmatrix} &= \begin{pmatrix} 0 \\ F_i^{f-rb} \end{pmatrix} \end{aligned} \tag{26}$$

$\mathbf{F}^{f-rb}$ are the fluid forces obtained by the force integration of the pressure and the viscous traction on the surface of the rigid body surface. Here, only one rigid body is considered. Generalizations to many of them is straightforward. Writing as a compact system:

$$\begin{aligned} \mathbf{M}_{rb}\frac{\mathrm{d}\mathbf{y}}{\mathrm{d}t} + \mathbf{A}_{rb}\mathbf{y} &= \mathbf{F}^{f-rb}(t,\mathbf{u}) \\ \mathbf{M}_{rb}\frac{\mathbf{y}^{n+1}-\mathbf{y}^n}{\Delta t} + \mathbf{A}_{rb}\mathbf{y}^{n+\alpha} &= \mathbf{F}^{f-rb}(t^{n+\alpha},\mathbf{u}^{n+\alpha}) \end{aligned} \tag{27}$$

with $\mathbf{y} = \begin{pmatrix} d_i \\ \dot{d}_i \end{pmatrix}$.

Both two way coupled systems are in general solved in a staggered way. In order to keep the second order accuracy in time of the global system a special rigid body displacement predictor is included. This predictor looks like:

$$\mathbf{d}^{(n+1)P} = \mathbf{d}^{(n)} + \alpha_0 \Delta t \dot{\mathbf{d}}^n + \alpha_1 \Delta t (\dot{\mathbf{d}}^n - \dot{\mathbf{d}}^{n-1}) \tag{28}$$

Figure 5 shows a simple numerical experiment where the role of the rigid body motion predictor is shown. The figure shows two bound straigh lines for first and second order accucary in time. The dots shown the following cases:

- monolithic (blue star) - 2nd order
- staggered with no predictor (black circle) - 1st order
- staggered with predictor $\alpha_0 = 1$ $\alpha_1 = 0$ (cyan star) - 1st order
- staggered with predictor $\alpha_0 = 1$ $\alpha_1 = \frac{1}{2}$ (red circle) - 2nd order

6 STRONGLY COUPLED PARTITIONED STAGED ALGORITHM

In this section the temporal algorithm that performs the coupling between the rigid body and the fluid codes is described. If the most outer loop (see the algorithm below), i.e. the 'stage loop' converges a *'strongly coupled'* algorithm is obtained. The basic staggered algorithm considered in this work proceeds as follows: (i) transfer the motion of the wet boundary of the rigid body to the fluid problem, (ii) update the position of the fluid boundary and the bulk fluid mesh accordingly, (iii) advance the fluid system and compute new pressures and the viscous stress field, (iv) convert the new fluid pressure and viscous stress field into a structural load, and (v) advance the rigid body system under the flow loads. Such a staggered procedure, which can be treated as a weakly coupled solution algorithm, can also be equipped with an outer loop in order to assure the convergence of the interaction process. The algorithm can be stated as follow:

1: Initialize variables:
2: **for** $n = 0$ to n_{step} **do** { *Main time step loop* }
3: $t^n = n\Delta t$,
4: { *CFD CODE:* }
5: $\mathbf{X}^n = \text{CMD}(\mathbf{d}^n)$ { *run CMD code* }
6: $\mathbf{d}^{(n+1)P} = \mathbf{d}^{(n+1,0)} = \text{predictor}(\mathbf{d}^n, \mathbf{d}^{n-1})$ { *compute predictor* }
7: **for** $i = 0$ to n_{stage} **do** { *stage loop* }
8: { *CFD CODE:* }
9: $\mathbf{X}^{n+1,i+1} = \text{CMD}(\mathbf{d}^{n+1,i})$
10: { *Compute skin normals and velocities* }
11: **for** $k = 0$ to n_{nwt} **do** { *Fluid Newton loop* }

```
      u^{n+1,i+1} = CFD(u^n, X^{n+1,i+1}, X^n)
    end for
    { Rigid body CODE: }
    compute structural loads (u^n, u^{n+1,i+1})
    { Integrate rigid body: }
    d^{n+1,i+1} = CMBD(d^n, u^n, u^{n+1,i+1})
  end for
end for
```

where

$\mathbf{u}^n$: is the fluid state $(\mathbf{v}, p)$ at time t^n,
$\mathbf{d}^n$: is the rigid body state (displacements) at time t^n,
$\dot{\mathbf{d}}^n$: are rigid body velocities at time t^n,
$\mathbf{X}^n$: are fluid mesh node positions at time t^n,
n_{step} : is the number of time steps in the simulation,
n_{stage} : is the number of stages in the coupling scheme
n_{nwt} : is the number of Newton loops in the nonlinear problem,
CMD : is intended for Computational Mesh Dynamics,
CMBD : for Computational Multibody Dynamics,
CFD : for Computational Fluid Dynamics.

6.1 Notes on the Fluid-Structure Interaction (FSI) algorithm

- Two codes (`CFD` and `CMBD`) are running simultaneously. For simplicity, the basic algorithm can be thought as if there were no *'concurrence'* between the codes, i.e. at a given time only one of them is running. This can be controlled using *'semaphores'* and this is done using MPI *'synchronization messages'*.
- The most external loop is over the time steps. Internal to it is the *'stage loop'*. *'Weak coupling'* is achieved if only one stage is performed (i.e. $n_{\text{stage}} = 1$). In each stage the fluid is first advanced using the previously computed multibody state $\mathbf{d}^n$ and the current estimate value $\mathbf{d}^{n+1,i}$.In this way, a new estimate for the fluid state $\mathbf{u}^{n+1,i+1}$ is computed. Next the multibody is updated using the forces of the fluid from states $\mathbf{u}^n$ and $\mathbf{u}^{n+1,i+1}$. At the first stage, the state $\mathbf{d}^{n+1,0}$ is predicted using a second or higher order approximation (see equation (30)). Inside the *stage loop* there is a Newton loop for the fluid code to solve the non-linearities. The Computational Multibody Dynamics (CSD) is integrated.
- Once the coordinates of the rigid body surfaces are known, the coordinates of the fluid mesh nodes are computed by a *'Computational Mesh Dynamics'* code, which is symbolized as

$$\mathbf{X}^n = \text{CMD}(\mathbf{d}^n). \tag{29}$$

Even though the CMD may be performed with a general strategy using both nodal reallocation or remeshing, in this paper only the former is adopted, keeping the topology unchanged. Relocation of mesh nodes can be done using an elastic or pseudo-elastic model (see Reference (Lopez et al., 2006)) through a separate PETSc-FEM parallel process (code named MESH-MOVE). For the simple geometry of the example in this paper a simple strategy is used based on a linear transformation of the rigid body displacement field.

- The general form of the predictor for the rigid body state was taken from Reference (Piperno and Farhat, 2001) and can be written as

$$\mathbf{d}^{(n+1)P} = \mathbf{d}^{(n)} + \alpha_0 \Delta t \dot{\mathbf{d}}^n + \alpha_1 \Delta t (\dot{\mathbf{d}}^n - \dot{\mathbf{d}}^{n-1}) \tag{30}$$

  It is at least first order accurate when no predictor is employed and it may be improved to second order using the above predictor with some values for α_0 and α_1 according to the problem at hand. To understand how to specify these two parameters a simple two *dofs* second order in time coupled ordinary differential equations model may be analyzed (Storti et al., 2006)
- At the beginning of each fluid stage there is a computation of skin normals and velocities. This is necessary due to the time dependent non-slip boundary condition for the incompressible flow solver (see equation (12)).

7 NUMERICAL EXAMPLES

In this section some validation for this application is done through standard benchmarks. The first example is the well known vortex-induced vibration around a cylinder at low Reynolds number, example well detailed in (Dettmer and Peric, 2006; Nomura and Hughes, 1992; Nomura, 1994) and references herein. The cylinder mounted on elastic supports is free to vibrate only in the vertical direction and it is immersed in a uniform flow field. The tank size is large enough to be regarded as infinite. Following the original data the dimensionless mass ratio is assigned to $m^* = 153.3524$, the structural damping coefficient is set to $\zeta = 0.5857$ and the frequency ratio is set to $F_n = 0.1766$.

Modifying the free stream velocity, starting from $Re = 90$ where the vortex shedding reaches a similar frequency to that obtained with a fixed cylinder, it is posible to cross across the lock-in region (around Re=100) where the vortex shedding is entrained with the oscillation natural frequency of the cylinder. Going further with greater values of Reynolds numbers (around 110), the oscillation becomes again desynchronizated making feasible to identify the lock-in region of this experiment. This narrow region depends on some dimensionless number. The following figure shows the geometry of the problem with the boundary conditions specified.

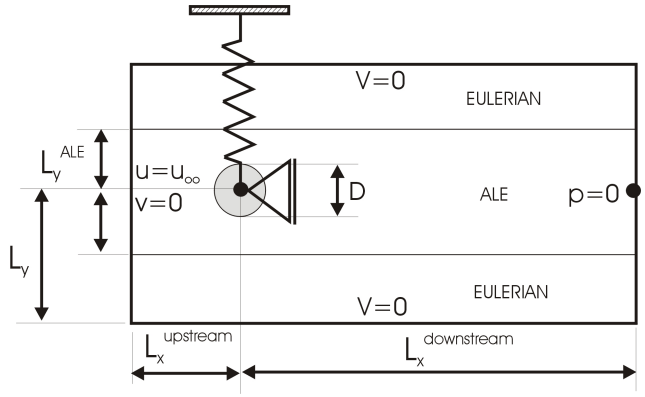

Figure 6: Description of test

The mesh used for this example is shown in figure 7. It has 3808 quadrilateral elements with 3940 nodes and, for illustrative purposes, it is plotted at a fictitious time step in order to magnify the deformation of the mesh. In general the maximum oscillation amplitude may be of the same order of the cylinder diameter. In Figure 6 the domain is split into two zones: an ALE zone

where the nodes of the mesh may be moved according to the rigid body surface motion and a region partitioned in a fix mesh. In this figure L_y is the half width of the domain and L_y^{ALE} is the half width of the ALE region. The ALE region moves in such a way to impose for the nodes at the interface between the rigid cylinder and the fluid the same velocity and for those at a specified distance from the cylinder a null velocity.

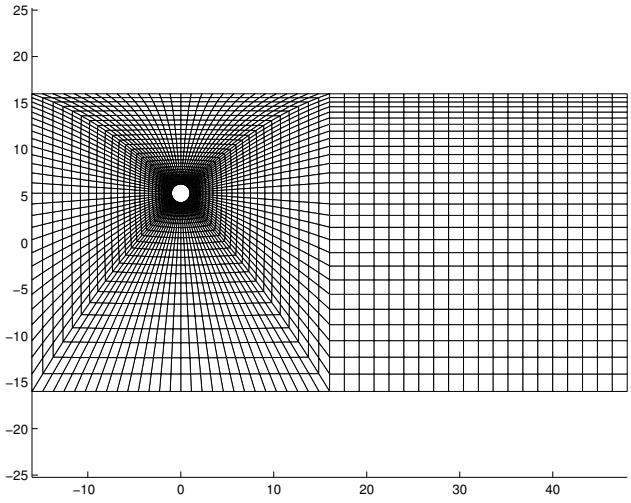

Figure 7: Mesh in a strongly deformed position

The characteristic behavior of this system is the lock-in phenomenon, there is an interval of free stream velocities for which the vortex shedding f_v agrees with the natural frequency f_n of the cylinder-spring-damper system. If U_∞ lies within this interval then the cylinder performs stable oscillations, with amplitudes as large as the cylinder diameter. Otherwise the oscillations are negligible. The existence of this lock-in region is an evidence of the two-ways coupling between the fluid and the mechanical systems. The fluid flow excites the oscillations of the cylinder, whereas the motion of the cylinder causes the lock-in effect altering the vortex shedding frequency f_v to be equal to the natural frequency f_n. This effect may be observed in the following figure 8. Detailed investigation of vortex-induced oscillations may be found in (Khalak and Williamson, 1999). The following list of dimensionless parameters fully specifies the problem.

- *mass ratio* $m^* = 153.3524$
- *frequency ratio* $F_n = 0.1766$
- *damping ratio* $\zeta = 0.5857$
- *Reynolds number* $Re \in (90, 150)$

They were chosen according to the reference (Dettmer and Peric, 2006).

In Figures 8 and 9 it may be noted that the present results are in good agreement with the numerical results obtained with the medium size mesh run by Dettmer and Peric (2006) and may be roughly similar with those presented by Nomura (Nomura and Hughes, 1992; Nomura, 1994). However the experimental results reported in (Dettmer and Peric, 2006) have some differences with the experimental ones, those reported in (Nomura and Hughes, 1992; Nomura, 1994). Here the former were included for some rough comparison.

Finer grid results, not included here for brevity reasons, agree very well with the finer grid results in (Dettmer and Peric, 2006), specially for the end of lock-in region when increasing Reynolds number. It is noted that while for coarser meshes the lock-in region is beyond Reynolds number $Re > 110$, finer grid results show that for $Re = 110$ the lock-in dissapears.

The next figures show how the cylinder oscillation develops in time for different Reynolds number. Also the phase between the oscillation and the vortex shedding is presented for the velocities involved. The vertical scales was modified in order to do both time evolutions comparable. Red curves are used for the vertical displacements and blue ones for forces.

It may be noted that for Reynolds numbers lower than the beginning of the lock-in fluid forces and cylinder oscillation are in phase with a very small oscillation amplitude. This pattern and the phase of the oscillation changes when the Reynolds lies in the lock-in region. Finally, when the synchronization is lost, the fluid forces and the cylinder oscillation remain with a phase difference of $\delta\phi = 180°$. This behavior was experimentally observed. This figures are taken after a periodic response was achieved.

Next figure shows how the lock-in pattern is reached since the beginning of the simulation, where the cylinder was left free to move and the fluid flow had reached its periodic behavior according to the Reynolds numbers involved.

8 CONCLUSIONS

Preliminary results for fluid-structure interaction with a rigid body cylinder was presented. Comparing with other equivalent numerical solutions, the lock-in phenomenon had been captured quite well. More work needs to be done to understand why the experimental observations show a wider lock-in region with Reynolds number. A sensitivity with structural parameters may be done to visualize how the experimental input data may influence the output results. For future it may be interesting to solve the in-line motion of the cylinder and investigate the hysteresis behavior with increasing and decreasing Reynolds number and its correlation with vortex-shedding modes and their jumps.

9 ACKNOWLEDGEMENTS

This work has received financial support from Consejo Nacional de Investigaciones Científicas y Técnicas (CONICET, Argentina, grants PIP-5271/2005), Universidad Nacional del Litoral (Argentina, grants CAI+D 2005-10-64) and ANPCyT (Argentina, grants PICT 12-14573/2003 (LAMBDA) , PME 209/2003 and PID 398/2003 (DIVA)). Extensive use of freely distributed software such as *GNU/Linux* OS, MPICH, PETSc, Metis, Octave, OpenDX and many others is done in this work.

REFERENCES

P. Bearman. Vortex shedding from oscillating bluff bodies. *Annual Review of Fluid Mechanics*, 16:195–222, 1984.

M. Behr. Stabilized space-time finite element formulations for free-surface flows. *Communications in Numerical Methods in Engineering*, 11:813–819, 2001.

T. Belytschko, D.R. Flanagan, and J.M. Kennedy. Finite element methods with user-controlled meshes for fluid-structure interaction. *Computer Methods in Applied Mechanics and Engineering*, 33:669–688, 1982.

R. Blevins. *Flow-induced vibrations*. Van Nostrand Reinhold, New York, 1990.

J. Cebral. *Loose Coupling Algorithms for fluid structure interaction*. PhD thesis, Institute for Computational Sciences and Informatics, George Mason University, 1996.

W. Dettmer and D. Peric. A computational framework for fluid-rigid body interaction: Finite element formulation and applications. *Comput Methods Appl Mech Engrg*, 195:1633–1666, 2006.

J. Donea, S. Giuliani, and J.P. Halleux. An arbitraty, lagrangian-eulerian finite element method for transient dynamic fluid-structure interactions. *Computer Methods in Applied Mechanics and Engineering*, 33:689–700, 1982.

E. Dowell, E. Crawley, H. Curtiss, D. Peters, R. Scanlan, and F. Sisto. *A Modern Course in Aeroelasticity*. Kluwer Academic Publishers, Dordrecht, 1995.

M. Facchinetti, E Langre, and F. Biolley. Coupling of structure and wake oscillators in vortex-induced vibrations. *Journal of Fluid and Structures*, 19:123–140, 2004.

R. Gabbai and H. Benaroya. An overview of modeling and experiments of vortex-induced vibration of circular cylinders. *Journal of Sound and Vibration*, 282:575–616, 2005.

O. Griffin and Ramberg S. Some recent studies of vortex shedding with applications to marine tubulars and risers. *Journal of Sound and Vibration*, 104:2–13, 1982.

I. Guler, M. Behr, and T. Tezduyar. Parallel finite element computation of free-surface flows. *Computational Mechanics*, 23:117–123, 1999.

T.J.R. Hughes, W.K. Liu, and T.K. Zimmermann. Lagrangian-eulerian finite element element formulation for incompressible viscous flows. *Computer Methods in Applied Mechanics and Engineering*, 29:239–349, 1981.

K. Jansen, C. Whiting, and Hulbert G. A generalized-α method for integrating the filtered navier-stokes equations with a stabilized finite element method. *Comput Methods Appl Mech Engrg*, 190:305–319, 2000.

A.A. Johnson and T.E. Tezduyar. Mesh update strategies in parallel finite element computations of flow problems with moving boundaries and interfaces. *Computer Methods in Applied Mechanics and Engineering*, 119:73–94, 1994.

A. Khalak and C. Williamson. Motions, forces and mode transitions in vortex-induced vibrations at low mass-damping. *Journal of Fluids and Structures*, 13:813–851, 1999.

E. Lopez, N. Nigro, M. Storti, and J. Toth. A minimal element distortion strategy for computational mesh dynamics. *Int J Num Meth Engng*, 2006.

Q. Lu, C. To, and Jin Z. Weak and strong interactions in vortex-induced resonant vibrations of cylindrical structures. *Journal of Sound and Vibration*, 190(5):791–820, 1996.

J. Meneghini and P. Bearman. Numerical simulation of high amplitude oscillatory flow about a circular cylinder. *Journal of Fluid and Structures*, 9:435–455, 1995.

S. Mittal and V. Kumar. Flow-induced vibrations of a light circular cylinder at reynolds numbers 10^3 to 10^4. *Journal of Sound and Vibration*, 245(5):923–946, 2001.

S. Mittal and T. Tezduyar. A finite element study of incompressible flows past oscillating cylinders and aerofoils. *Int. J. for Num. Meth. in Fluids*, 15:1073–1118, 1992.

E. Naudascher and Rockwell. *Flow induced Vibrations: An Engineering Guide.* Balkema, Rotterdam, 1993.

T. Nomura. Ale finite element computations of fluid structure interaction problems. *Comput Methods Appl Mech Engrg*, 112:291–308, 1994.

T. Nomura and T. Hughes. An arbitrary lagrangian-eulerian finite element method for interaction of fluid and a rigid body. *Comput Methods Appl Mech Engrg*, 95:115–138, 1992.

G. Parkinson. Phenomena and modelling of flo-induced vibrations of bluff bodies. *Progress in Aerospace Sciences*, 26:169–224, 1989.

R. Piperno and C. Farhat. Partitioned procedures for the transient solution of coupled aeroelastic problems. Part II: energy transfer analysis and three-dimensional applications. *Comput Methods Appl Mech Engrg*, 190:3147–3170, 2001.

T. Sarpkaya. Vortex-induced oscillations. *Journal of Applied Mechanics*, 46:241–258, 1979.

F. Shakib. *Finite element analysis of the compressible Euler and Navier-Stokes equations*. PhD thesis, Department of Mechanical Engineering, Stanford University, 1989.

S. Singh and S. Mittal. Vortex-induced oscillations at low reynolds numbers: Hysteresis and vortex-shedding modes. *Journal of Fluids and Structures*, 20:1085–1104, 2005.

M. Storti, N. Nigro, and R. Paz. Stability and time integration of partitioned fluid-structure interaction problems at supersonic mach numbers. *Journal of Sound and Vibration*, 0:1–1, 2006.

B. Sumer and J. Fredsoze. *Hydrodynamics around cylindrical structures*. World Scientific, Singapore, 1997.

T. Tezduyar, M. Behr, S. Mittal, and A. Johnson. Computation of unsteady incompressible flows with the stabilized finite element methods–space-time formulations, iterative strategies and massively parallel implementations. In *New Methods in Transient Analysis*, PVP-VOL.246/AMS-Vol.143, pages 7–24. ASME, New York, 1992a.

T. Tezduyar, S. Mittal, S. Ray, and R. Shih. Incompressible flow computations with stabilized bilinear and linear equal order interpolation velocity pressure elements. *Computer Methods in Applied Mechanics and Engineering*, 95:221–242, 1992b.

T. Tezduyar, S. Sathe, R. Keedy, and K. Stein. Space-time techniques for finite element computation of flows with moving boundaries and interfaces. In *III Congreso Internacional sobre Métodos Numéricos en Ingeniería y Ciencias Aplicadas*, 2004.

T. E. Tezduyar. Stabilized finite element formulations for incompressible flow computations. *Advances in Applied Mechanics*, 28:1–44, 1992.

T. E. Tezduyar, M. Behr, and J. Liou. A new strategy for finite element computations involving moving boundaries and interfaces - the deforming-spatial-domain/space-time procedure: I. the concept and the preliminary numerical tests. *Computer Methods in Applied Mechanics and Engineering*, 94:339–351, 1992c.

T. E. Tezduyar, M. Behr, S. Mittal, and J. Liou. A new strategy for finite element computations involving moving boundaries and interfaces - the deforming-spatial-domain/space-time procedure: Ii. computation of free-surface flows, two-liquid flows, and flows with drifting cylinders. *Computer Methods in Applied Mechanics and Engineering*, 94:353–371, 1992d.

T. E. Tezduyar, S. Sathe, R. Keedy, and K. Stein. Space-time finite element techniques for computation of fluid-structure interactions. *Computer Methods in Applied Mechanics and Engineering*, 195:2002–2027, 2006.

T.E. Tezduyar and Y.J. Park. Discontinuity capturing finite element formulations for nonlinear convection-diffusion-reaction equations. *Computer Methods in Applied Mechanics and Engineering*, 59:307–325, 1986.

K. Vikestad, J. Vandiver, and C. Larsen. Added mass and oscillation frequency for a circular cylinder subjected to vortex-induced vibrations and external disturbance. *Journal of Fluid and Structures*, 14:1071–1088, 2000.

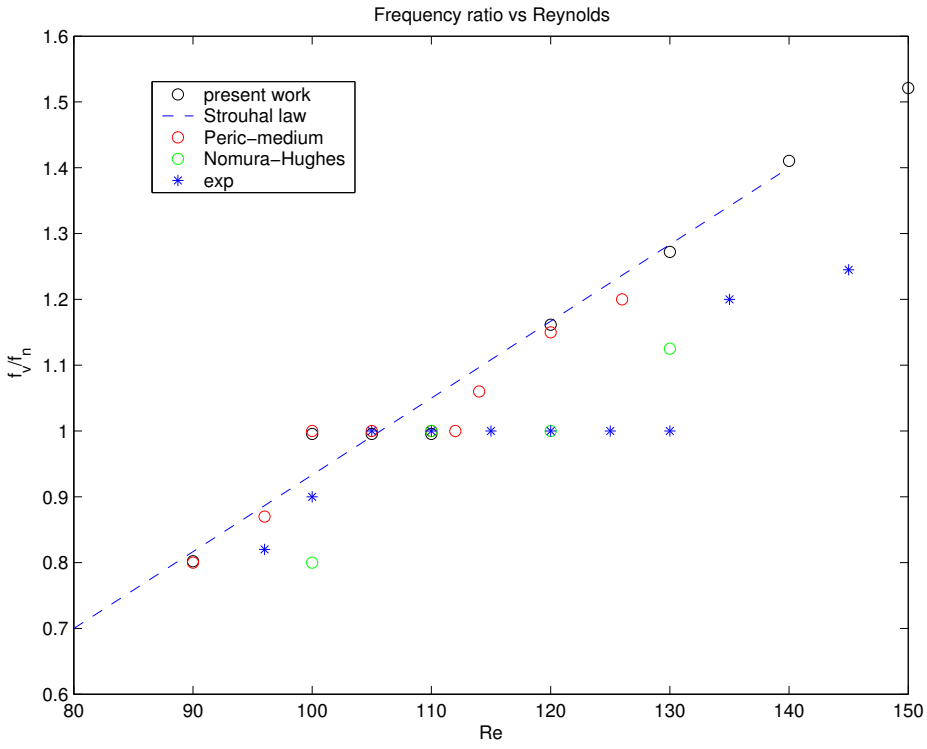

Figure 8: Frequency ratio versus Reynolds number - Comparisons between numerical and experimental results.

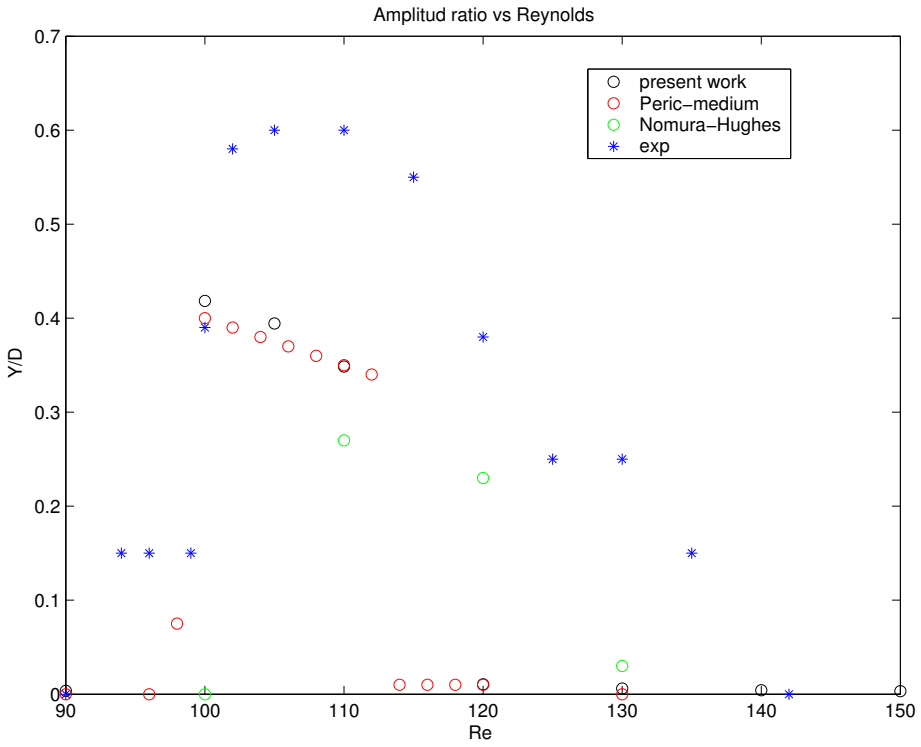

Figure 9: Amplitude ratio versus Reynolds number - Comparisons between numerical and experimental results.

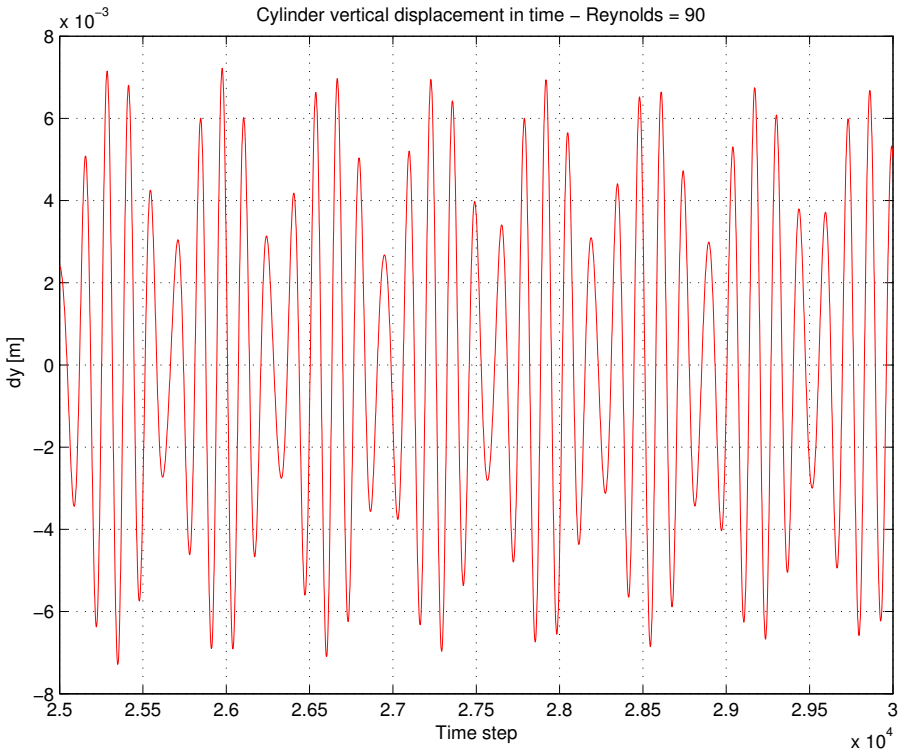

Figure 10: Periodic time response of the cylinder oscillation amplitude. $Re = 90$

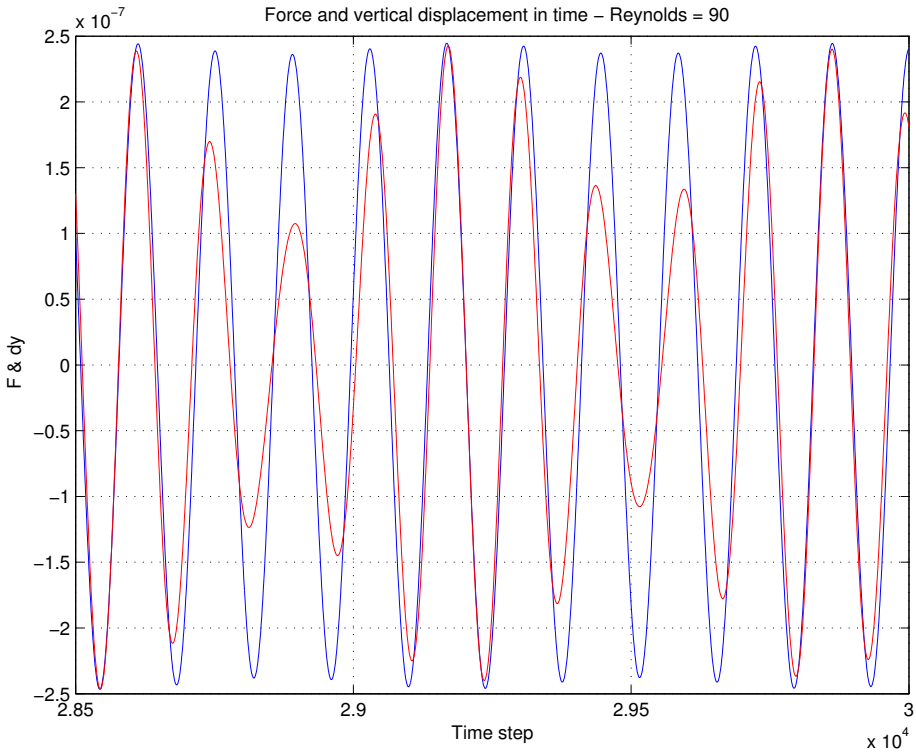

Figure 11: Periodic time response of the phase between the cylinder oscillation and the vortex shedding. $Re = 90$

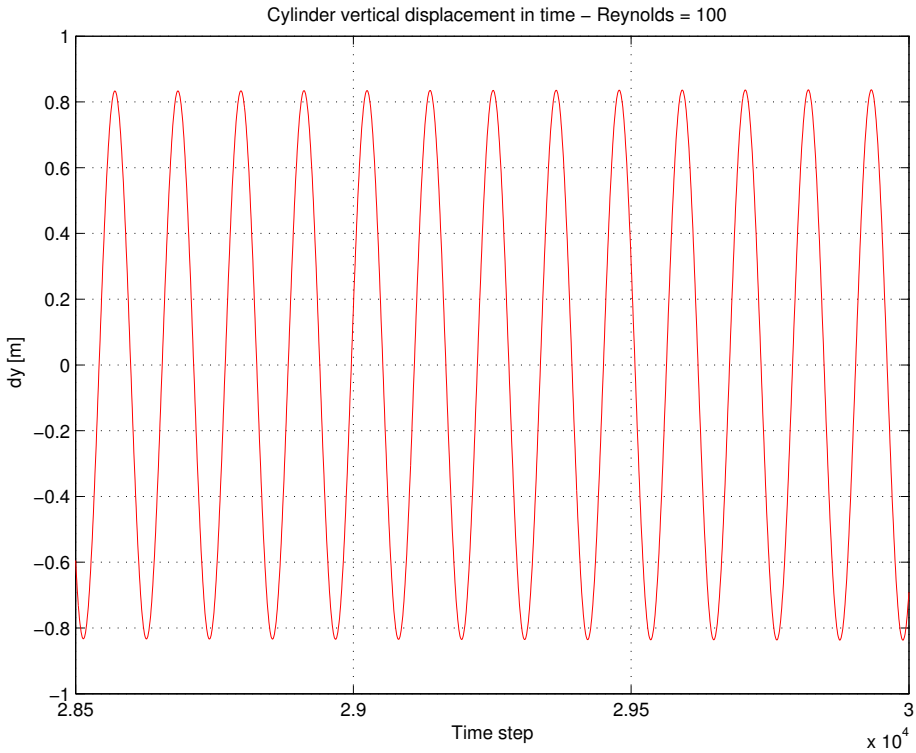

Figure 12: Periodic time response of the cylinder oscillation amplitude. $Re = 100$

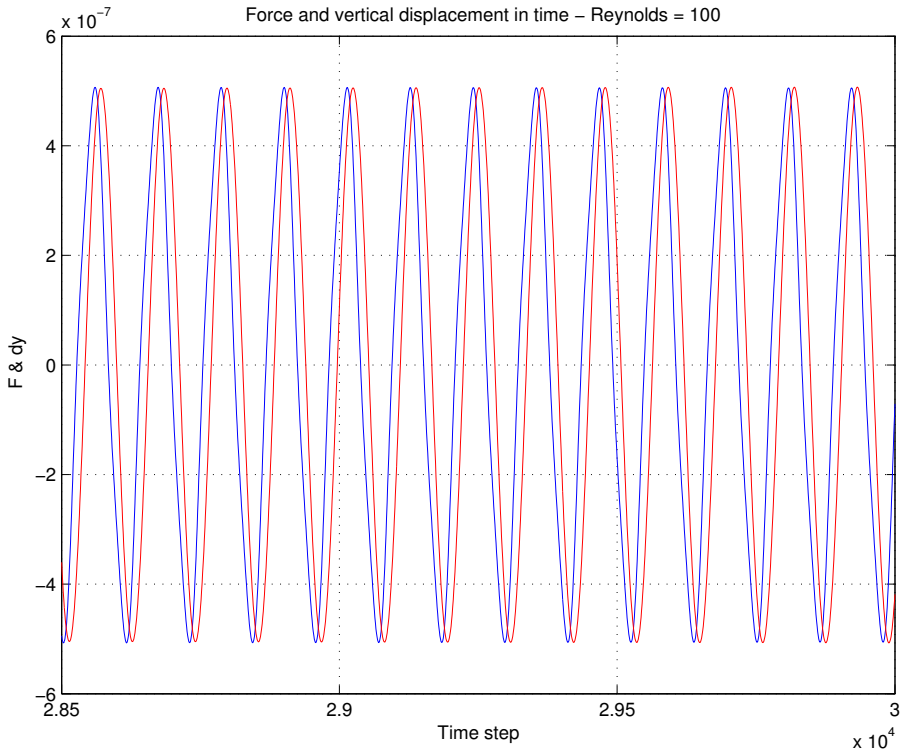

Figure 13: Periodic time response of the phase between the cylinder oscillation and the vortex shedding. $Re = 100$

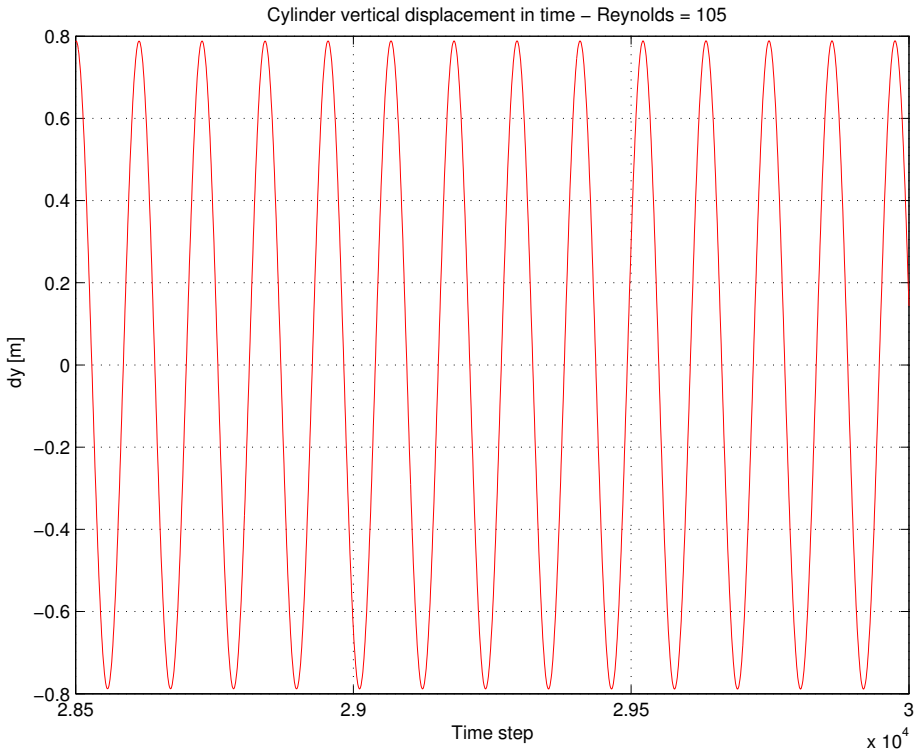

Figure 14: Periodic time response of the cylinder oscillation amplitude. $Re = 105$

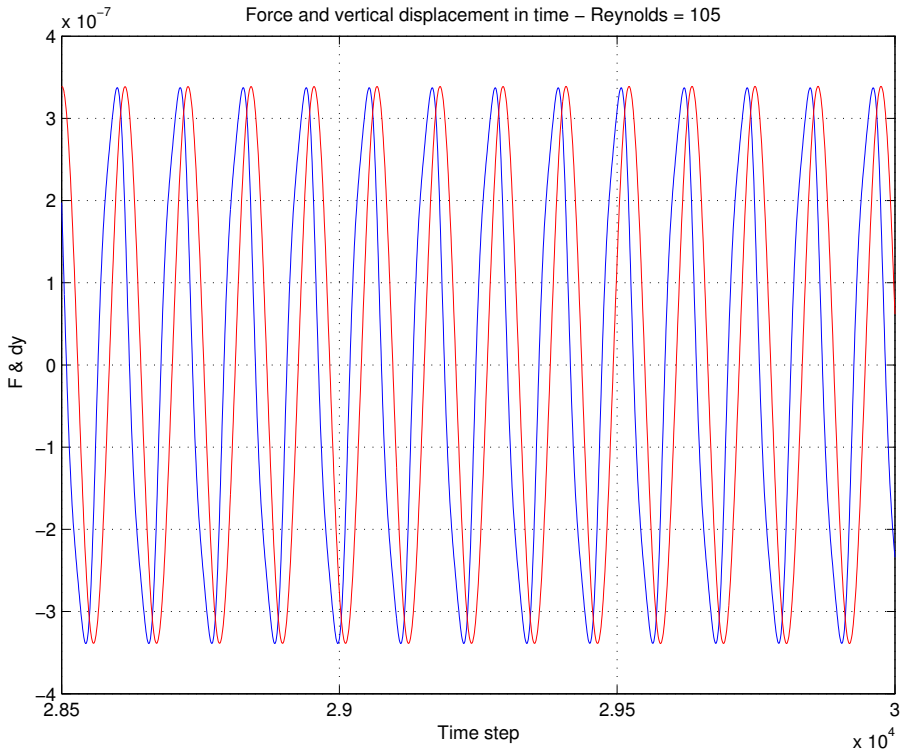

Figure 15: Periodic time response of the phase between the cylinder oscillation and the vortex shedding. $Re = 105$

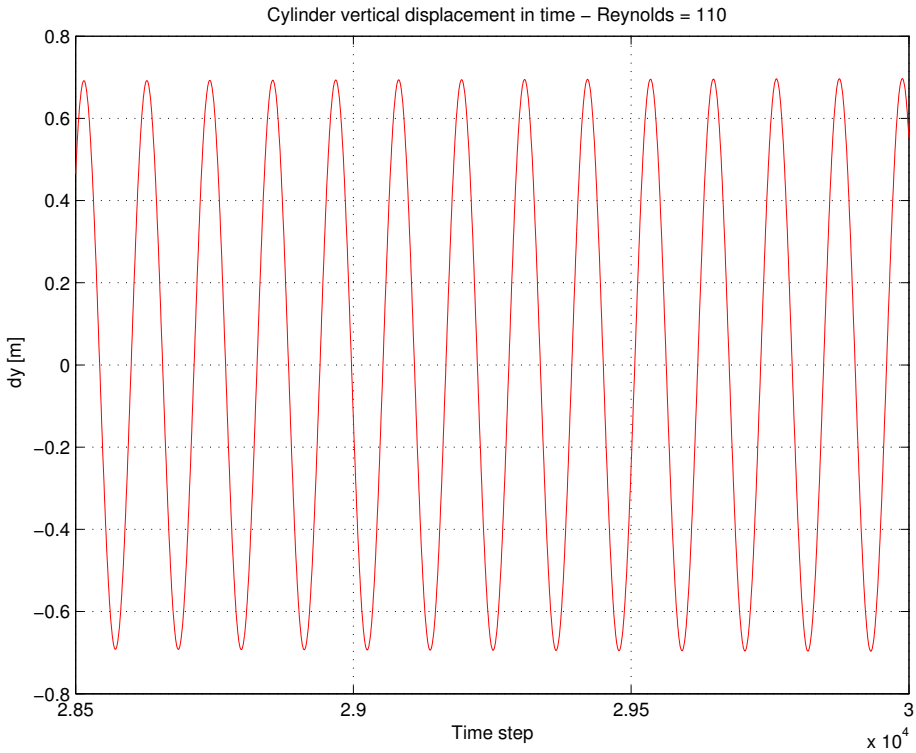

Figure 16: Periodic time response of the cylinder oscillation amplitude. $Re = 110$

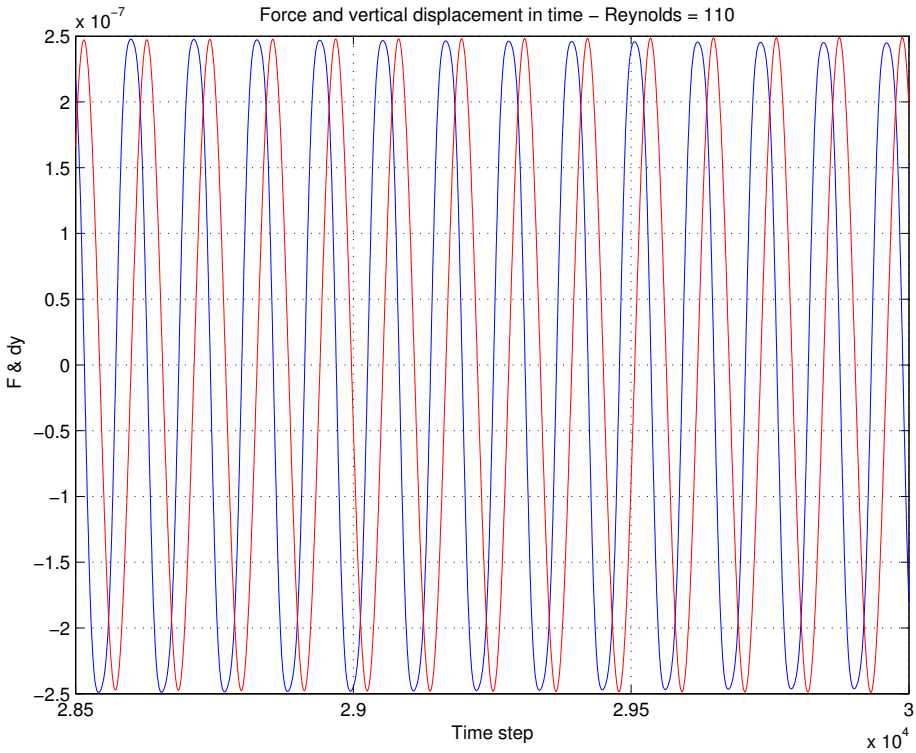

Figure 17: Periodic time response of the phase between the cylinder oscillation and the vortex shedding. $Re = 110$

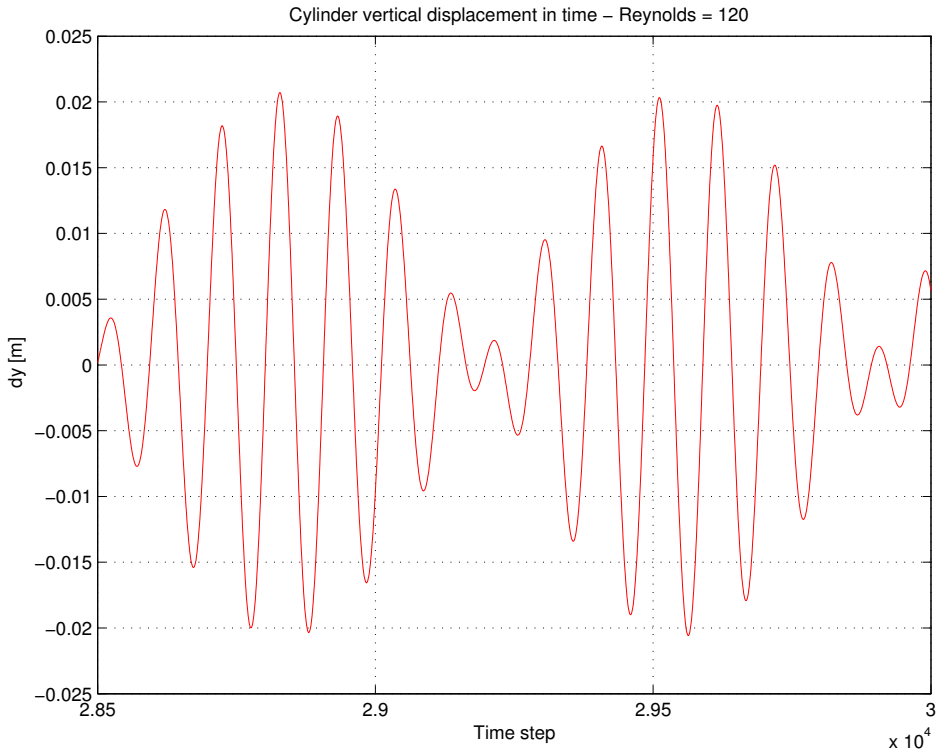

Figure 18: Periodic time response of the cylinder oscillation amplitude. $Re = 120$

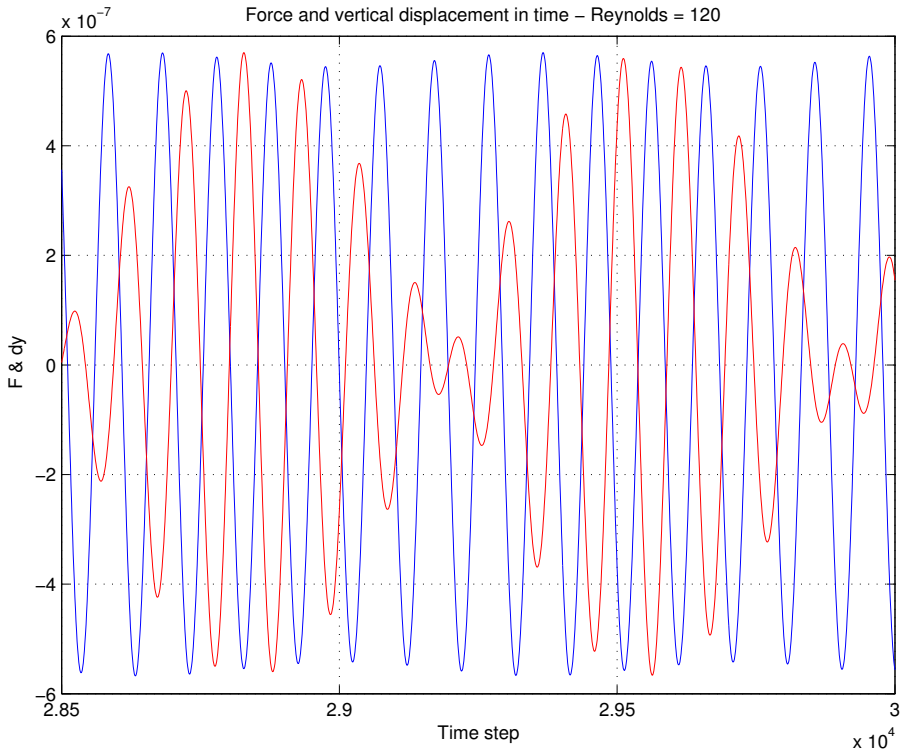

Figure 19: Periodic time response of the phase between the cylinder oscillation and the vortex shedding. $Re = 120$

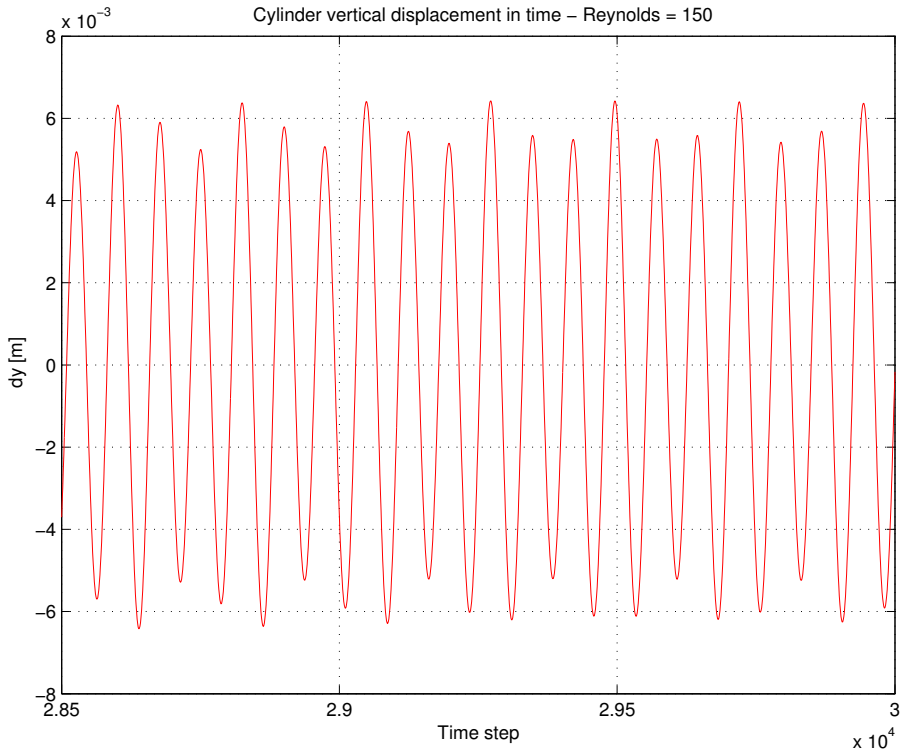

Figure 20: Periodic time response of the cylinder oscillation amplitude. $Re = 150$

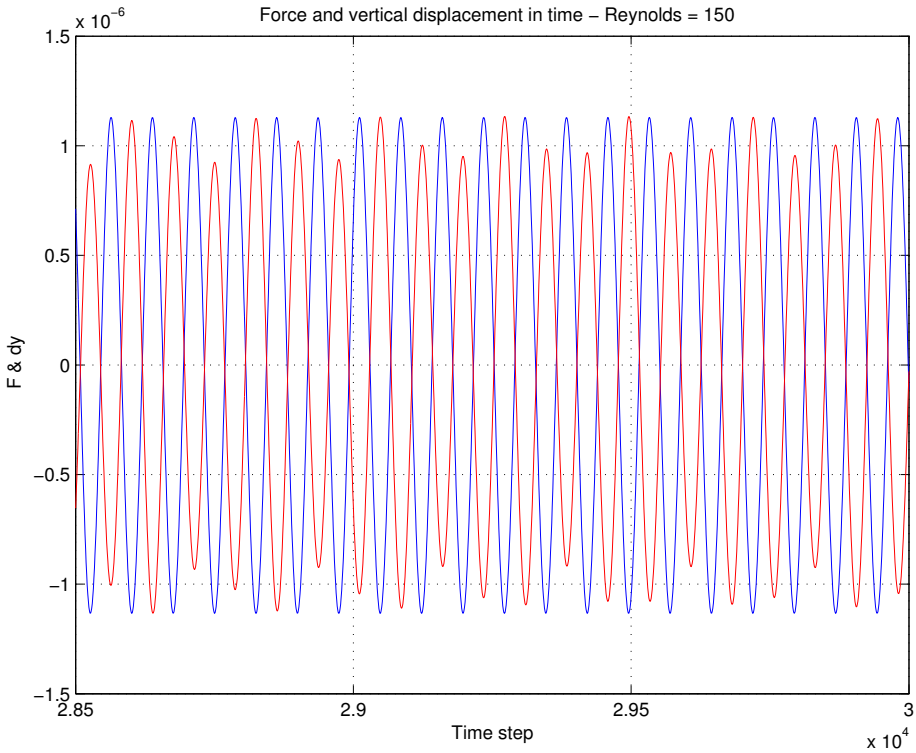

Figure 21: Periodic time response of the phase between the cylinder oscillation and the vortex shedding. $Re = 150$

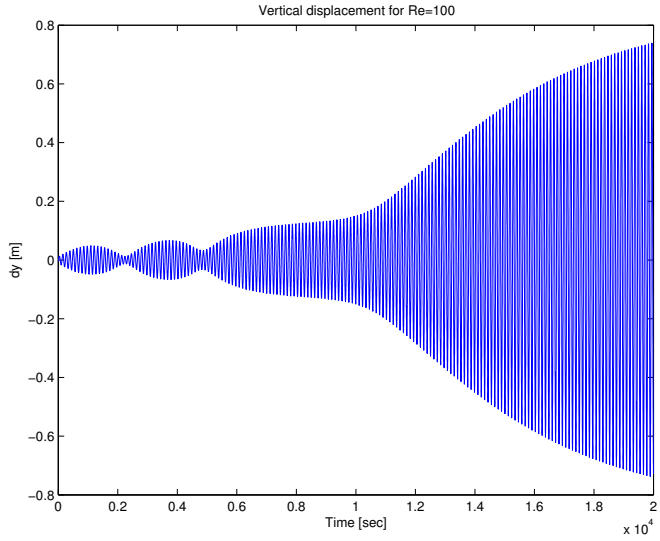

Figure 22: Time response of the cylinder oscillation amplitude from the beginning for Reynolds number belonging to the lock-in region . $Re = 100$